Hydrologic response of catchments to precipitation: Quantification of mechanical carriers and origins of water

Y.-J. Park,[1] E. A. Sudicky,[1] A. E. Brookfield,[1,2] and J. P. Jones[1]

[1] Precipitation-induced overland and groundwater flow and mixing processes are quantified to analyze the temporal (event and pre-event water) and spatial (groundwater discharge and overland runoff) origins of water entering a stream. Using a distributed-parameter control volume finite-element simulator that can simultaneously solve the fully coupled partial differential equations describing 2-D Manning and 3-D Darcian flow and advective-dispersive transport, mechanical flow (driven by hydraulic potential) and tracer-based hydrograph separation (driven by dispersive mixing as well as mechanical flow) are simulated in response to precipitation events in two cross sections oriented parallel and perpendicular to a stream. The results indicate that as precipitation becomes more intense, the subsurface mechanical flow contributions tend to become less significant relative to the total pre-event stream discharge. Hydrodynamic mixing can play an important role in enhancing pre-event tracer signals in the stream. This implies that temporally tagged chemical signals introduced into surface-subsurface flow systems from precipitation may not be strong enough to detect the changes in the subsurface flow system. It is concluded that diffusive/dispersive mixing, capillary fringe groundwater ridging, and macropore flow can influence the temporal sources of water in the stream, but any sole mechanism may not fully explain the strong pre-event water discharge. Further investigations of the influence of heterogeneity, residence time, geomorphology, and root zone processes are required to confirm the conclusions of this study.

1. Introduction

[2] During a precipitation event, new water is introduced into a hydrological system where it mixes with old water and flows. Hydrograph separation techniques are commonly used to deduce temporal sources of stream discharge by tracing unique chemical signals that existed before (pre-event water) or are introduced during a precipitation event (event water). It may not be appropriate to directly relate these temporally tagged tracer signals to spatial sources of stream discharge [*McGlynn and McDonnell*, 2003; *Jones et al.*, 2006; *Renaud et al.*, 2007; *Sudicky et al.*, 2007]. For example, a greater proportion of pre-event water in stream discharge does not necessarily represent stronger Darcian groundwater inputs. It was indicated by *Renaud et al.* [2007] and *Sudicky et al.* [2007] that some statements and terminologies in the literature are somewhat ambiguous as to the temporal sources of water versus the mechanical carriers of water (for details, see *Jones et al.* [2006], *Renaud et al.* [2007], and *Sudicky et al.* [2007]). For example, pre-event tracer signals are often interpreted as riparian

groundwater "runoff," generated by precipitation events [e.g., *Burns et al.*, 2001; *Weiler et al.*, 1999], and this rapid mobilization of groundwater was referred to as an old-water paradox for stormflow generation [*Kirchner*, 2003].

[3] The hydrological response to a precipitation event can be interpreted as a purely mechanical flow process, where water migrates from higher to lower hydraulic potential, such as in the solution of the mass balance partial differential equations based on Manning surface flow and Darcian subsurface flow. It is noted that these mechanical processes do not include mixing processes such as diffusion and mechanical dispersion. The arguments of *Renaud et al.* [2007] and *Sudicky et al.* [2007] can be clarified by stating that the tracer technique for hydrograph separation to deduce the temporal origins of water entering a stream is influenced not only by pure mechanical flow processes, but also by mixing processes induced by chemical potential gradients. Although precipitation falls on the land surface, a portion can flow overland, while some infiltrates such that the overland and groundwater flow components entering a stream may carry both event and pre-event waters. *Jones et al.* [2006] compared the event and pre-event contributions to stream discharge with and without hydrodynamic dispersion (molecular diffusion and mechanical dispersion) and indicated that mixing processes could play an important role in determining tracer signals in the stream. *McGlynn and McDonnell* [2003] attempted to directly measure and compare the temporal (old and new) and spatial (riparian

---

[1]Department of Earth and Environmental Sciences, University of Waterloo, Waterloo, Ontario, Canada.
[2]Now at Kansas Geological Survey, University of Kansas, Lawrence, Kansas, USA.

and hillslope) sources of catchment runoff. *Botter et al.* [2010] derived a generalized formulation for the lumped hydrological response (travel-time probability density) of catchments to precipitation and suggested that various eco-hydrological processes taking place in the soil could influence the travel-time distribution of water and solutes in river basins. *Botter et al.* [2010] also indicated that mixing processes between old and new water are likely to occur in the soil during flushing episodes triggered by floods and that these processes are key factors affecting the shape of travel-time probability density functions.

[4] Following *Renaud et al.* [2007] and *Sudicky et al.* [2007], it is necessary to further clarify and quantify the relationship between temporally tagged tracer signals and pure mechanical flow processes. Approaches that use chemical signals to determine mechanical flow components are well established for traditional tracer tests: For example, a migrating plume originating from a tracer signal introduced into the system as a pulse is monitored to estimate the mechanical water velocity and the degree of mixing (dispersion). Note that the irreversible mixing process increases the entropy of the system by eventually making the spatial and temporal signals uniform. Thus, if the input signal (source concentration) is relatively weak compared to the travel time, the results may not be readily interpreted. Likewise, it is desirable to compare the strength of the input signals with the strength of mixing processes in order to determine the relation that the temporal origins of water in the stream may have with pure mechanical flow processes.

[5] In this study, mechanical flow and mixing processes occurring during and after a precipitation event are illustrated and quantified in a simplified catchment by applying a fully integrated surface-subsurface model to two cross sections oriented parallel and perpendicular to a stream. The HydroGeoSphere simulator used in this study is a comprehensive, fully integrated, physically based, and distributed-parameter numerical model that can simultaneously solve the partial differential equations describing three-dimensional variably saturated subsurface Darcian flow and two-dimensional Manning overland/streamflow and advective-dispersive solute transport [*Therrien et al.*, 2003]. It has been demonstrated that the fully integrated approach can be successfully applied to hydrologic systems at various scales for a variety of purposes by eliminating the artificial boundary condition at the surface-subsurface interface which is unavoidable for abstracted surface or subsurface models [*Loague and VanderKwaak*, 2002, 2004; *Loague et al.*, 2005., 2006; *Jones et al.*, 2006, 2008; *Ebel et al.*, 2007a, 2007b; *Li et al.*, 2008; *Sudicky et al.*, 2008; *Brookfield et al.*, 2009]. For example, fluxes are seamlessly passed between the surface and subsurface flow regimes to simulate the entire land phase of the hydrologic cycle. The main objective of this study is to provide insight into how precipitation influences the flow field in a catchment, how water of different temporal origins is redistributed during and after precipitation, and to analyze the relationship between the spatial and temporal origins of stormflow in the stream. Factors that can affect groundwater flow patterns during precipitation and the manner in which mechanical dispersion and molecular diffusion can alter input precipitation signals is quantified and demonstrated with a series of numerical examples.

2. Processes Occurring Along a Stream

[6] Figure 1a shows the distribution of surface and subsurface water in an example catchment. In Figure 1a, surface water flows toward topographically low regions, being generated by precipitation (stormflow) while groundwater flows from regions of high- to low-hydraulic potential forms base flow to the streams between precipitation events. The subsurface water table is a subdued replica of the topography, thus generating groundwater flow from topographic highs to lows [*Tóth*, 1963]. In a schematic catchment, as shown in Figure 1b, the dominant hydrological processes consist of streamflow and saturated groundwater flow beneath the stream in plane A (as illustrated in the left side of Figure 2a); while infiltration from the surface to the subsurface, percolation through the unsaturated zone, saturated groundwater flow, and the development of a seepage face are the main processes occurring in plane B (as illustrated in the right side of Figure 2a). Other processes such as evaporation and transpiration are excluded in this study for clarity and simplicity because of the short time frames under consideration (<10 h). Note that the simplifications made for the simulations, such as the exclusion of hyporheic zone details, and uniformity and isotropy of hydraulic
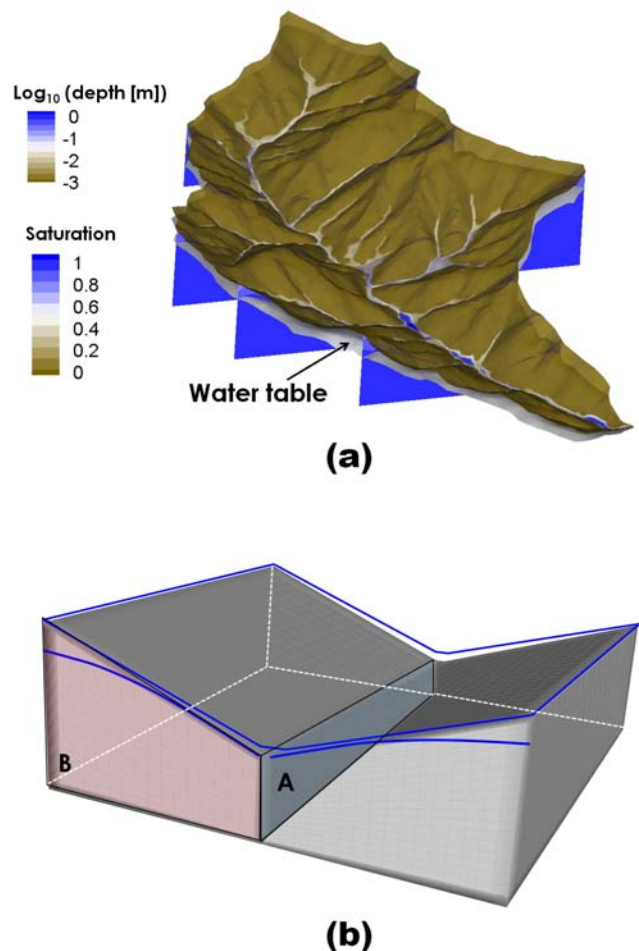

Figure 1. (a) Surface and subsurface water distribution in an example catchment and (b) a schematic illustration of a watershed for further numerical analysis.
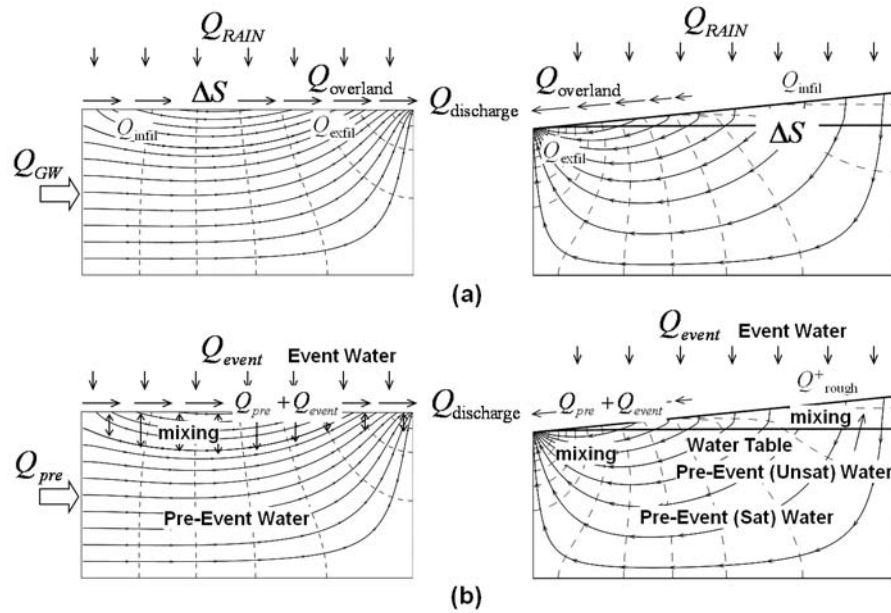
Figure 2. (a) Mechanistic processes during a precipitation event and (b) the origins of water molecules with mixing processes. The left column illustrates the processes in a cross section along the stream (plane A), while the right shows processes in a section across the stream (plane B).

properties, may influence the results within relatively dynamic surficial flow regime or even for regional-scale hydrology; and thus the simulation results can be best interpreted in terms of relative distinction between flow regimes and the relative strength in the influence by various physical and chemical mechanisms for stormflow generation.

2.1. Mechanical Flow Driven by Precipitation and Tracer-Based Hydrograph Separation: Plane A Results

[7] For the schematic hillslope setting along plane A of Figure 1b, the two-dimensional vertical cross-sectional

subsurface domain (20 m long and 10 m deep) was discretized using 250,000 (4 cm × 2 cm) rectangular elements and the one-dimensional overland flow domain was discretized using 500 4 cm linear elements. Streamflow was generated by a specified rainfall flux over the land surface, which has a mild topographic slope of 0.0025 (5 cm over 20 m length). Groundwater flows into the domain from the left specified head boundary ($H = 10$ m), and both surface and subsurface flow components discharged at the downstream end of the stream where a critical-depth boundary condition was applied (Figure 3a). A hydraulic conductivity of 10^{-5} m s^{-1}
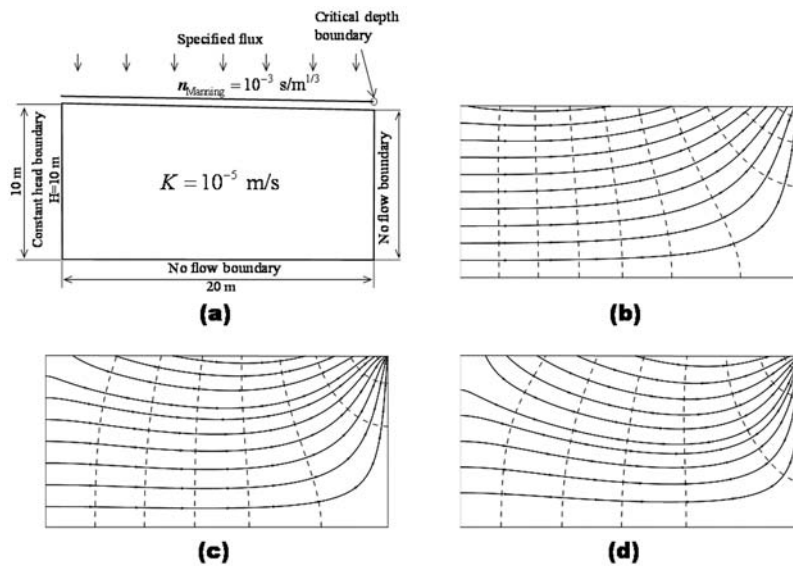

Figure 3. Illustration of the enhanced groundwater flow due to precipitation events in (a) the conceptual modeling domain for plane A in Figure 1b. Q_{event} = (b) 2 mm h^{-1}, (c) 10 mm h^{-1}, and (d) 20 mm h^{-1}.

(based on the measured values for fine to medium grained sand at the Borden aquifer, Ontario, Canada [*Sudicky*, 1986; *Turcke and Kueper*, 1996]) and a Manning's roughness coefficient of 0.001 s m$^{-1/3}$ were assigned for the subsurface porous medium and the overland flow domains, respectively (for details, see Figure 1 and Table 1 by *Jones et al.* [2006]). A steady state flow system was first established by applying a precipitation rate of 1 mm d^{-1}, which was then used as an initial condition to simulate the response following storm events. It is noted that the subsurface domain is always saturated for the given initial and boundary conditions, although the HydroGeoSphere model [*Therrien et al.*, 2003] allows an unsaturated zone to develop. Figures 3b–3d show the patterns of streamlines that develop in the subsurface at the end of a 1 h precipitation event for three different rates equal to 2, 10, and 20 mm h^{-1}. It is clear in Figure 3 that more intense precipitation events can generate a greater amount of throughflow (often referred to as "piston flow"), which becomes stronger compared to the initial ambient groundwater flow.

[8] In order to quantify the subsurface flow component (a mechanical carrier as described by Darcy's law) that is enhanced by the precipitation events, groundwater inflow integrated along the left specified head boundary (Q_{GW}) and the infiltration from the surface to subsurface (Q_{infil}) are calculated and averaged over the event period (Table 1). In Table 1, $\bar{Q}$ represents an average over the event period (T : 1 h) such that $\bar{Q} = \int_T Q dt / T$. Note that if the subsurface is saturated, the exfiltration from the subsurface to the overland domain (Q_{exfil}) can be calculated from the sum of the infiltration and the groundwater inflow ($Q_{\mathrm{exfil}} = Q_{\mathrm{infil}} + Q_{GW}$). The results provided in Figure 3 and Table 1 indicate that as the precipitation ($\bar{Q}_{\mathrm{event}}$) becomes more intensive, event-induced throughflow ($\bar{Q}_{\mathrm{infil}}$) becomes stronger compared to the ambient groundwater flow ($\bar{Q}_{GW}$); however, both subsurface flow components are relatively small compared to the total stream discharge ($\bar{Q}_{\mathrm{discharge}}$). It is noted in Table 1 that the difference between precipitation water applied to the system ($\bar{Q}_{\mathrm{event}}$) and the total stream discharge ($\bar{Q}_{\mathrm{discharge}}$) contributes to the increase of the water storage overwhelmingly in the surface flow domain.

[9] The temporal origins of water in the stream discharge, as interpreted from a tracer-based hydrograph separation technique, can be easily examined using the integrated flow and transport model: the rainfall containing a unit concentration of a dissolved conservative tracer ($C_{\mathrm{event}} = 1$) is applied to the land surface. Because the initial condition consists of zero concentration in the entire surface and subsurface domains ($C_{\mathrm{event}}[t = 0] = 0$), the simulated concentrations at any time and location ($C_{\mathrm{event}}[\mathbf{x}, t]$) can be interpreted as the event water fraction. Therefore, the event water fraction computed in the stream and multiplied by the stream discharge ($Q_{\mathrm{discharge}}$) represents the event water contribution to the stream discharge ($\bar{Q}_{\mathrm{discharge}}^{\mathrm{event}} = \int_T Q_{\mathrm{discharge}} C_{\mathrm{event}} dt / T$). In the context of transport, the process of hydrodynamic dispersion must be considered. It is noted that hydrodynamic dispersion as defined by *Bear* [1972] refers to additive processes of Fickian molecular diffusion and mechanical dispersion, and the Fickian hydrodynamic dispersion process is assumed for transport in the surface as well as in the subsurface:

$$\theta_s D_{ij} = (\alpha_L - \alpha_T) \frac{q_i q_j}{|q|} + \alpha_T |q| \delta_{ij} + \tau \theta_s D_{\mathrm{free}} \delta_{ij}, \qquad (1)$$

where θ_s is the saturated water content or porosity, D is the hydrodynamic dispersion tensor, α_L and α_T are the longitudinal and transverse dispersivities, q is the specific discharge, and δ_{ij} is the Kronecker delta. For this and all subsequent simulations, constant longitudinal and transverse dispersivity values of 1.0 and 0.1 m [*Schwartz and Zhang*, 2003] are used and the saturated effective molecular diffusion coefficient ($D_e = \theta_s \tau D_{\mathrm{free}}$) equals 4.44×10^{-10} m^2 s^{-1} (porosity, $\theta_s = 0.37$, tortuosity $\tau = 1$ for simplicity, and free solution diffusion coefficient $D_{\mathrm{free}} = 1.2 \times 10^{-9}$ m^2 s^{-1}). The transport simulation results describing the temporal origins of water in the stream discharge ($\bar{Q}_{\mathrm{discharge}}^{\mathrm{event}}$ and $\bar{Q}_{\mathrm{discharge}}^{\mathrm{pre\text{-}event}}$ as summarized in Table 1) show that the pre-event contribution becomes far greater than the mechanical subsurface flow components ($\bar{Q}_{GW}$ and $\bar{Q}_{\mathrm{infil}}$) and the ratio $\bar{Q}_{\mathrm{discharge}}^{\mathrm{pre\text{-}event}} / \bar{Q}_{\mathrm{discharge}}^{\mathrm{event}}$ becomes smaller with more intense precipitation, which is consistent with the simulation results by *Jones et al.* [2006]. Thus, the strong pre-event stream discharge often deduced from conventional tracer-based hydrograph separations can be ascribed to the added effects of diffusion and mechanical dispersion, but not only to "piston flow" or the changes in subsurface flow patterns as shown in Figure 3.

2.2. Effects of Macropore Flow

[10] Flow through macropores and the potentially rapid transmission of pre-event water to a stream has been postulated as an important physical mechanism to account for strong pre-event signals observed in streams [*McDonnell*, 1990; *Weiler and Naef*, 2003]. An integrated surface water and dual-permeability subsurface flow model [*VanderKwaak*, 1999; *Therrien et al.*, 2003] can be used to assess the effects of macropores on the flow field and the redistribution of event and pre-event water in the two-dimensional cross sections shown in Figure 3a. In general, the dual-permeability approach conceptualizes the soil matrix and macropores as two overlapping continua [*Barenblatt et al.*, 1960; *Gerke and van Genuchten*, 1993; *Larsbo et al.*, 2005]. The macropores can transmit a significant amount of water due to their higher hydraulic conductivity compared to the soil matrix,

Table 1. Precipitation-Induced Surface and Subsurface Flow Along With Temporal Sources of Stream Discharge[a]

Conceptual Model	$\bar{Q}_{\mathrm{event}}$	$\bar{Q}_{\mathrm{discharge}}$	$\bar{Q}_{\mathrm{discharge}}^{\mathrm{event}}$	$\bar{Q}_{\mathrm{discharge}}^{\mathrm{pre\text{-}event}}$	$\bar{Q}_{GW}$	$\bar{Q}_{\mathrm{infil}}$
Single continuum	40	0.69	0.13	0.56	0.83	0.03
	200	47.4	31.8	15.6	0.65	0.26
	400	150.8	121.7	29.1	0.53	0.50
Dual continuum	40	5.06	1.35	3.71	6.22	0.34
	200	54.4	36.2	18.2	4.76	1.17
	400	140.0	111.4	28.6	3.55	1.91

[a]The stream discharge is at the outlet point of the system shown in Figure 3a for plane A for three different precipitation events (L h^{-1}). Values are averaged over the precipitation period (1 h).

but compose only a small fraction of the bulk porosity of the medium. A detailed description of the approach can be found in *VanderKwaak* [1999] or *Therrien et al.* [2003].

[11] Simulations similar to those performed in section 2.1 will now be carried out, but the domain given by plane A is taken to contain a macropore continuum where the saturated hydraulic conductivity of the macropore system is set to equal to 7.2×10^{-3} m s^{-1} and only 1% of the bulk volume fraction is occupied by the macropores. The soil matrix has the same hydraulic and transport properties (hydraulic conductivity equal to 1.0×10^{-5} m s^{-1} and a porosity of 0.37) as used in section 2.1. The dual-continuum results provided in Table 1 show that both subsurface mechanical flow components ($\bar{Q}_{GW}$ and $\bar{Q}_{\text{infil}}$) become stronger compared to the results for the single-continuum cases because the bulk hydraulic conductivity is larger with macropores present. However, as the precipitation becomes more intense, both of these macropore-enhanced mechanical components remain significantly less than the total pre-event discharge to the stream, $\bar{Q}_{\text{discharge}}^{\text{pre-event}}$ (mechanical plus dispersive mixing), as was the case in single-continuum simulations.

[12] Figure 4 shows the distribution of the event water fraction in the soil matrix and the macropore continua at the end of the 1 h precipitation event with a rate of 10 mm h^{-1}. The results shown in Figure 4 indicate that the initial pre-event water in the shallow region of the macropore continuum is readily replaced by event water because it is more conductive and contains only a small volume fraction. Because the ambient groundwater flow ($\bar{Q}_{GW}$) is also enhanced by the macropore continuum, event and pre-event water mixing is stronger near the groundwater discharge outlet at the top right of the cross section. In conclusion, macropores can enhance the subsurface flow and the mixing processes; for more intensive precipitation, the macropore-enhanced mechanical flow becomes relatively insignificant compared to the pre-event contribution to the stream discharge which includes both mechanical and dispersive inputs. Compared to single-continuum simulation cases, pre-event water contributes more to the total stream discharge because of the enhanced mechanical input of water and because of the enhanced dispersive input to the stream induced by the macropores.

3. Processes Occurring Across the Stream: Plane B Results

[13] Precipitation applied to the land surface either flows over the land surface or infiltrates into the subsurface. Depending on the strength and duration of the precipitation event, the infiltrated water can reach the water table zone as recharge to the saturated zone. Hydrological processes occurring in the subsurface domain perpendicular to a stream (plane B of Figure 1b) are illustrated in the right column of Figure 2. It is shown in Figure 2 that vertical flow is dominant in the unsaturated zone until the water infiltrated from the surface reaches the capillary fringe. Saturated groundwater flows from topographic highs to lows, where a seepage face is developed. Residence time in the subsurface is relatively short near the seepage face and thus the region adjacent to the stream is hydrologically more active compared to the remainder of the subsurface domain. *Sklash and Farvolden* [1979] and *Gillham* [1984] suggested that rain-induced groundwater ridging in media containing a relatively thick, but shallow, capillary fringe could account for the rapid mobilization of groundwater and the high proportion of pre-event water contributing to stream discharge. *Cloke et al.* [2006] showed that this hypothesis might hold only in certain limited environments.

3.1. Mechanical Response to a Precipitation Event

[14] For the schematic hillslope settings along plane B of Figure 1b, the slope of the land surface was assumed to be steeper (0.1) than the case for plane A described in section 2. All of the material properties are taken to be same as in section 2.1 and the parameters appearing in the van Genuchten retention relation for unsaturated flow are taken from *Jones et al.* [2006] for Borden sand. For the simulation of storm events, an initial condition is established by applying precipitation at a rate of 1 mm d^{-1} until steady state is achieved (Figure 5). The side and bottom boundaries are zero flux and water is allowed to discharge on the upper left surface representing the stream.

[15] Figure 6 shows the fluctuation of the water table and the change in the saturation distribution during a precipitation event. A 10 mm h^{-1} rate of precipitation is applied to the surface domain for 1 h and the response of the surface and subsurface is then simulated for 5 h. Capillary-fringe
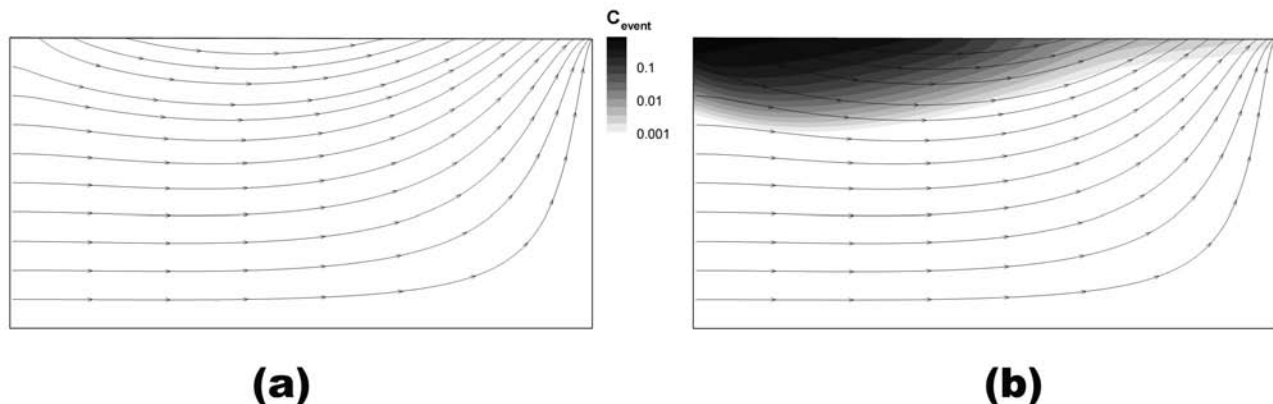

(a)   **(b)**

Figure 4. Distribution of event water for plane A in the (a) soil matrix and (b) macropore continua at the end of a 1 h precipitation event when $Q_{\text{event}} = 10$ mm h^{-1}.
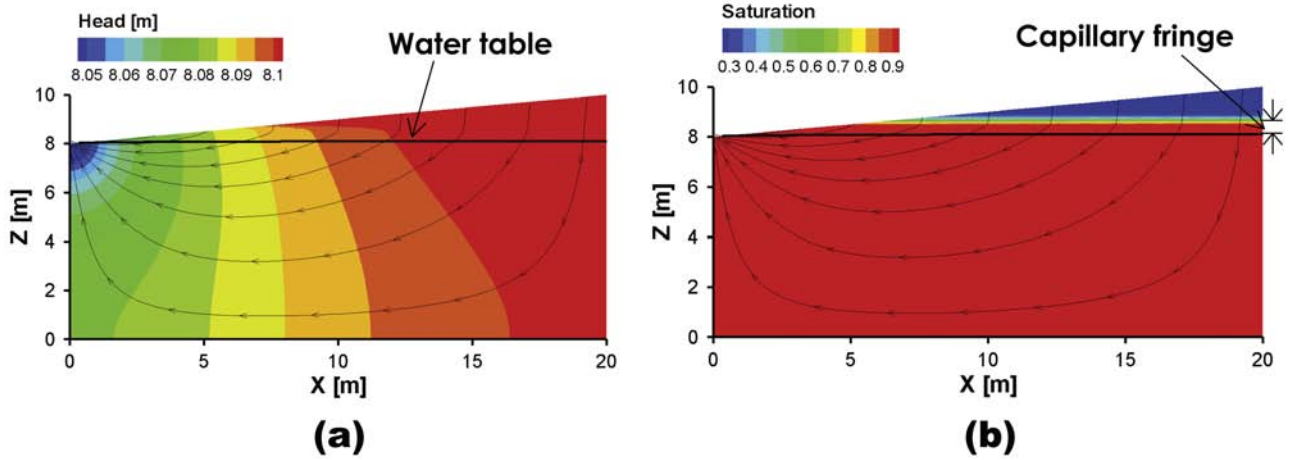
Figure 5. Hillslope hydrological conditions in the subsurface domain for plane B of Figure 2b: (5a) flow net and (5b) saturation distribution.

groundwater ridging can be seen near the stream in Figure 6. In Figure 6, the water table rises up to the ground surface almost instantaneously after the start of the event where the groundwater table is close to ground surface. In the remainder of the domain, the hydrological response is relatively slow, without any significant change. Figure 7 shows the streamlines near the stream and the distribution of groundwater flux during the simulation. The results indicate that the hydraulic response is limited to the shallow region near the stream and the infiltration process in the uphill region is relatively slow. The observed capillary-fringe groundwater ridging is comparable to field and simulation results found
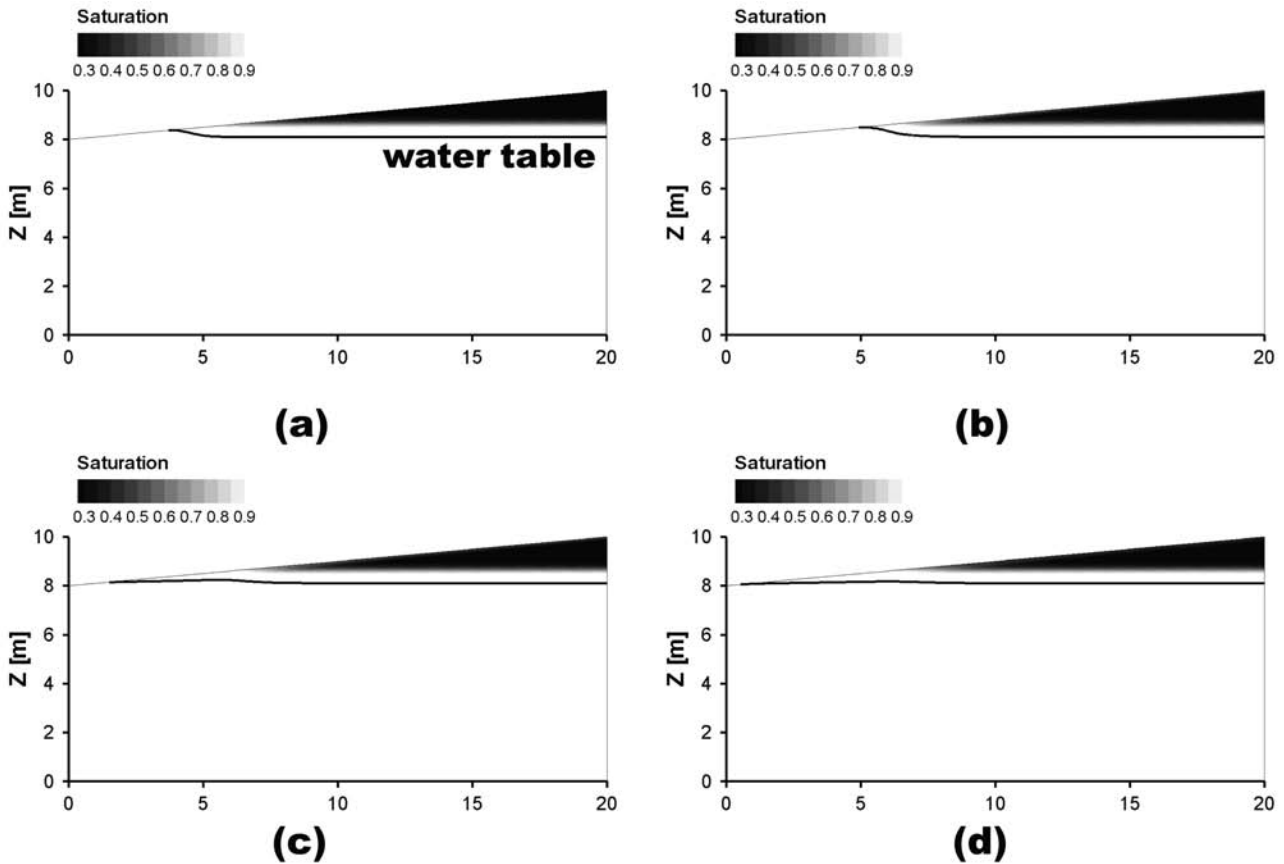

Figure 6. Hydrological response in the schematic hillslope for plane B during a precipitation event: water table location and saturation distribution (a) 10 min and (b) 1 h after the start of precipitation, and (c) 10 min and (d) 1 h after precipitation stops.
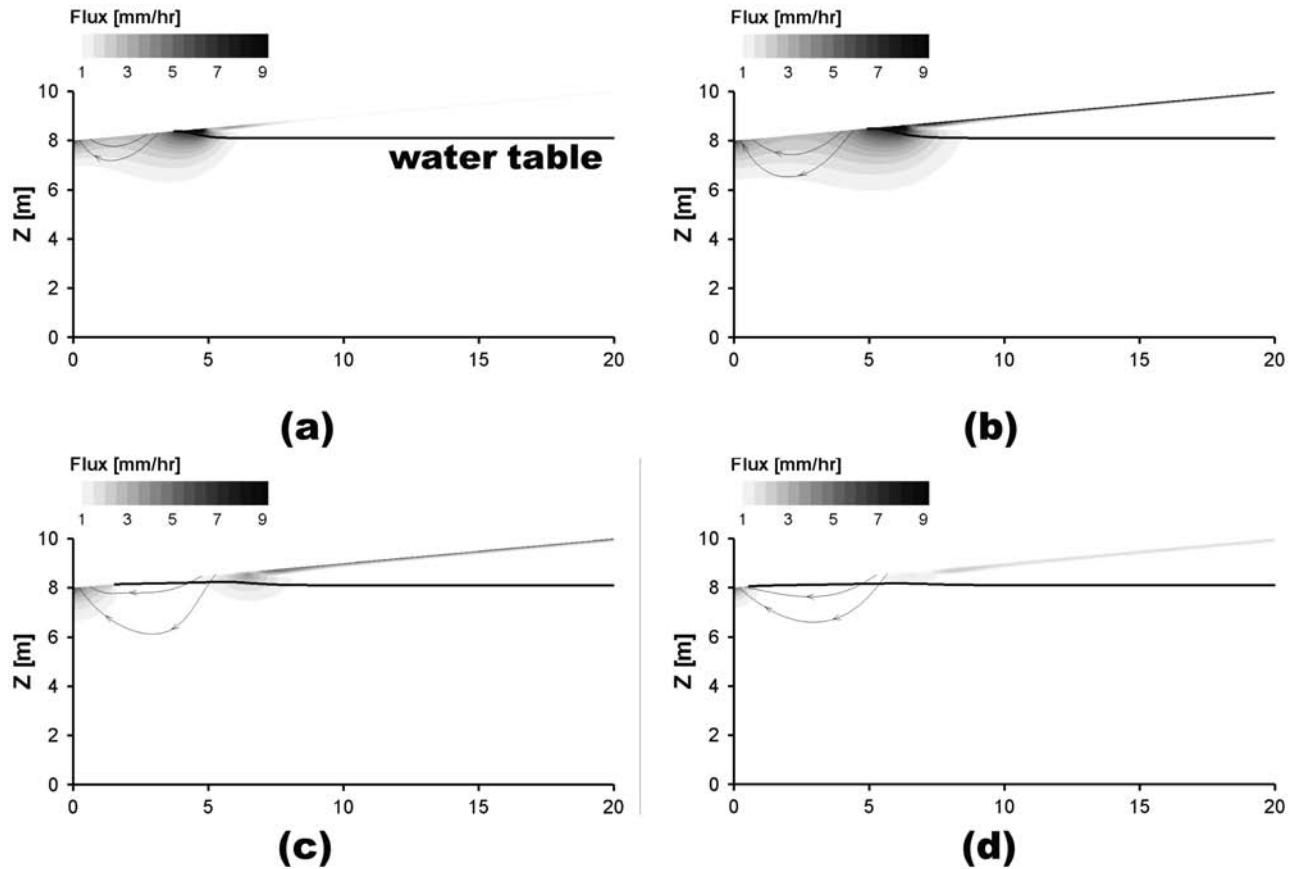
Figure 7. Hydrological response in the schematic hillslope for plane B during a precipitation event: streamlines and groundwater flux distribution (a) 10 min and (b) 1 h after the start of precipitation, and (c) 10 min and (d) 1 h after precipitation stops.

in the literature [e.g., *Abdul and Gillham*, 1989; *Cloke et al.*, 2006].

[16] Table 2 summarizes the mechanical flow components and the temporal origins of water at the outlet of the hillslope, in response to three different precipitation rates. During the precipitation event, most of the water applied to the land surface infiltrates into the subsurface ($\bar{Q}_{infil}$). As the precipitation becomes more intensive, the ratio between infiltration to precipitation ($\bar{Q}_{infil}/\bar{Q}_{event}$) decreases due to stronger capillary-fringe groundwater ridging that generates greater infiltration-excess overland flow. The amount of exfiltration ($\bar{Q}_{exfil}$, the flow from the subsurface to the surface) is comparable to the stream discharge (59%) for the case with the lowest precipitation rate. As the precipitation

rate increases, however, exfiltration contributes less to the stream discharge (13% and 6% for the 10 and 20 mm h^{-1} precipitation cases, respectively).

3.2. Temporal Origin of Water: Pre-Event and Event Water

[17] Here the migration of three conservative hypothetical tracers is simulated to tag precipitation event water and pre-event waters in the saturated and unsaturated zones. The concentration of the event water tracer is initially zero in the domain (both surface and subsurface regimes), but is assigned a value of unity in the event water that is applied to the overland domain as precipitation. The concentration of the pre-event saturated zone tracer is initially unity in

Table 2. Precipitation-Induced Surface and Subsurface Flow Along With Temporal Sources of Stream Discharge[a]

Conceptual Model	$\bar{Q}_{event}$	$\bar{Q}_{discharge}$	$\bar{Q}_{discharge}^{event}$	$\bar{Q}_{discharge}^{pre-event(sat)}$	$\bar{Q}_{discharge}^{pre-event(unsat)}$	$\bar{Q}_{infil}$	$\bar{Q}_{exfil}$
Single continuum	40	4.13	0.53	2.72	0.88	31.9	2.44
	200	32.5	13.0	11.9	7.6	153.4	4.16
	400	75.6	42.6	19.2	13.8	272.0	4.29
Dual continuum	40	3.67	0.47	1.85	1.35	31.9	3.46
	200	22.8	10.4	6.8	5.6	170.1	16.0
	400	55.1	34.7	11.0	9.4	331.5	26.8

[a]The stream discharge is at the outlet point of the system shown in Figure 5 for plane B for three different precipitation events (L h^{-1}). Values are averaged over the precipitation period (1 h).

the saturated subsurface (zero elsewhere), and the tracer concentration of the pre-event water in the unsaturated zone is initially unity but is zero in the saturated portion of the subsurface prior to applying the precipitation. Simulated concentrations for these three independent tracers at the downstream end of the stream represent the event water, the pre-event saturated, and pre-event unsaturated water contributions ($\bar{Q}_{\mathrm{discharge}}^{\mathrm{event}}$, $\bar{Q}_{\mathrm{discharge}}^{\mathrm{pre\text{-}event(sat)}}$, and $\bar{Q}_{\mathrm{discharge}}^{\mathrm{pre\text{-}event(unsat)}}$) when they are multiplied by the total stream discharge and averaged over the event period as summarized in Table 2 (for details describing the hydrograph separation methodology used here, see *VanderKwaak* [1999] and *Jones et al.* [2006]).

[18] In Table 1, the amount of exfiltration ($\bar{Q}_{\mathrm{exfil}}$, mechanical flow from the subsurface to the surface) is comparable to the total pre-event water discharge (68%) for the case with the lowest precipitation rate. However, as precipitation becomes more intense, the exfiltration, $\bar{Q}_{\mathrm{exfil}}$, becomes less significant compared to the total pre-event water discharge (21% and 13% for the 10 and 20 mm h^{-1} precipitation cases, respectively). It is interesting to note that as the rain intensity and capillary-fringe groundwater ridging become stronger, the contribution of the pre-event stream discharge from the unsaturated zone becomes larger relative to the saturated component: the $\bar{Q}_{\mathrm{discharge}}^{\mathrm{pre\text{-}event(unsat)}}/\bar{Q}_{\mathrm{discharge}}^{\mathrm{pre\text{-}event(sat)}}$ values are 32%, 64%, and 72% for the three cases. These results, combined with the exfiltration rates, imply that capillary-fringe groundwater ridging may not generate enough mechanical flow to the stream to account for the observed pre-event stream discharge [*Cloke et al.*, 2006], but it may accelerate mixing processes such that more pre-event water discharges to the stream.

[19] Figure 8 shows the event water distribution in the subsurface at the end of the precipitation event ($t = 1.0$ h). By excluding hydrodynamic dispersion, event water moves solely by mechanical flow that is driven by gravity, pressure gradients, and capillary tension. It should be noted that a fine mesh and a total variation diminishing (TVD)-type

flux limiter is used in HydroGeoSphere to minimize numerical dispersion during advection-dominated transport [*van Leer*, 1974; *Unger et al.*, 1996]. The results in Figure 8c confirm that event water moves primarily by vertical gravity-driven flow and capillarity in the unsaturated region and its distribution is limited to the near surface region of the subsurface domain. Molecular diffusion and mechanical dispersion enhance the mixing of event and pre-event water near the discharge zone along the seepage face (Figures 8a and 8b).

[20] The temporal origin of water at the discharge point (located at the top left corner of the domain) is provided in Figure 9. The results shown in Figure 9 indicate that both molecular diffusion and mechanical mixing are important mechanisms to consider when determining the origin of water. The pre-event water contribution by mechanical flow processes to the stream discharge is limited without dispersion.

[21] The total discharge over the 5 h of simulation time was calculated to be about 45 L of the total 200 L of applied precipitation, with the remainder of the water simply increasing the storage in the system. The results imply that a significant amount of event water slowly reaches the saturated zone and ultimately discharges to the stream through the saturated zone, thus contributing to the stream's base flow. In Figures 8 and 9, it is shown that event water infiltration is a relatively slow process compared to the stream response and that the base flow to the stream is maintained by the pre-event water that existed in the saturated zone (dashed lines in Figure 9).

3.3. Event Water Diffusion Into the Subsurface

[22] The purely diffusive exchange of event and pre-event waters (e.g., tagged water molecules) between surface and subsurface is illustrated here using a simple analytical solution to the one-dimensional diffusion equation. The overland domain ($z = 0$) is assumed to contain purely event water during the event and the subsurface ($z > 0$) is initially composed of pre-event water. By considering only diffusion,
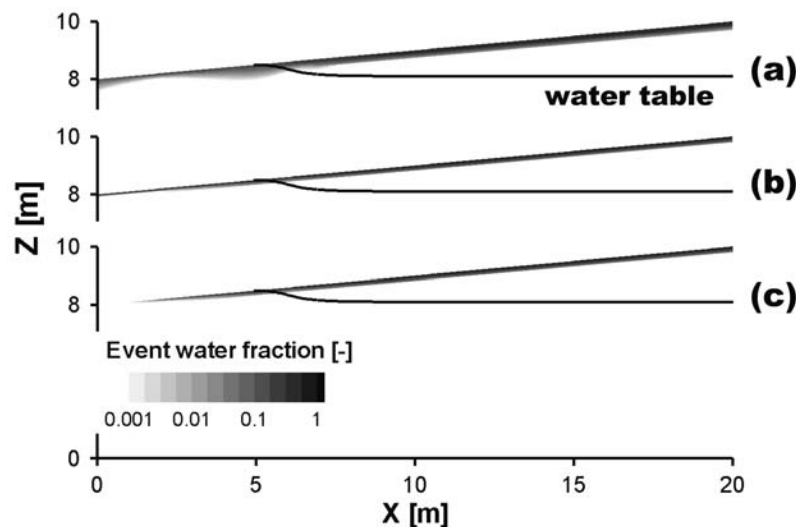

Figure 8. Event water distribution after precipitation ends ($t = 1.0$ h) for plane B: (a) with molecular and mechanical mixing, (b) with only molecular mixing, and (c) without dispersion.
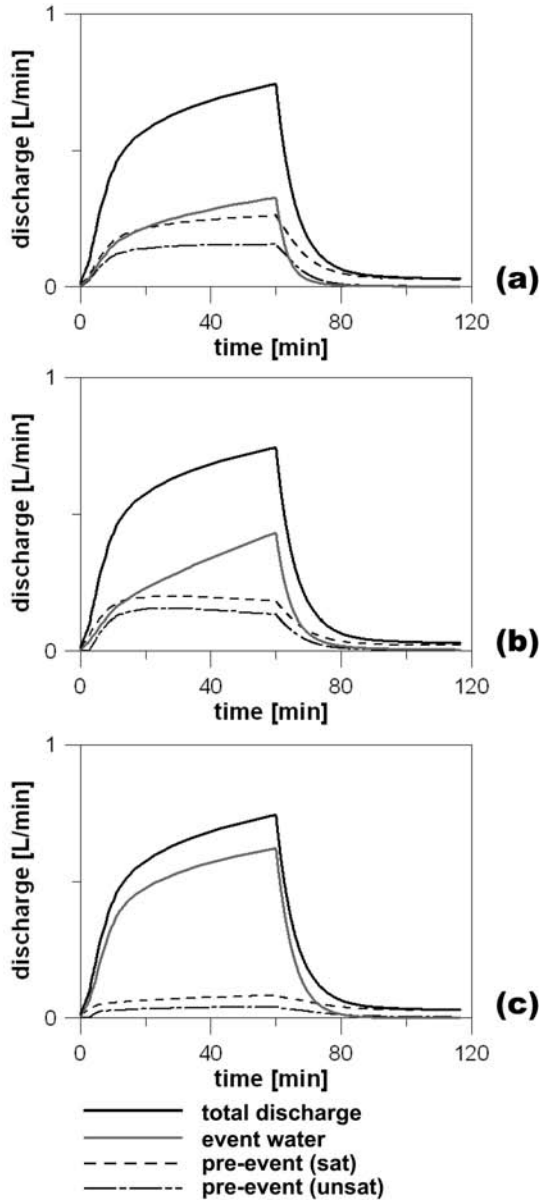
Figure 9. Origins of water in the discharge point for plane B: (a) with molecular and mechanical mixing, (b) with only molecular mixing, and (c) without dispersion.

the concentration of event water (C_{event}) in the semi-infinite subsurface domain can be determined from a solution to the following equation with the given initial and boundary conditions:

$$\frac{\partial C_{\text{event}}}{\partial t} = D_e \frac{\partial^2 C_{\text{event}}}{\partial z^2}, \qquad (2a)$$

$$C_{\text{event}}(z, t = 0) = 0, \qquad (2b)$$

$$C_{\text{event}}(z = 0, t) = 1, \qquad (2c)$$

where D_e is the effective diffusion coefficient, $D_e = \theta_s S_w \tau D_{\text{free}}$ for a given porosity θ_s, water saturation

S_w, tortuosity τ, and free-solution diffusion coefficient D_{free} [*Domenico and Schwartz*, 1998]. It is noted that diffusion in general, is not limited to the vertical direction but the concentration gradient is assumed to be effectively one-dimensional in the example calculations. The solution for (2) is

$$C_{\text{event}}(z, t) = \text{erfc}\left[\frac{z}{\sqrt{4 D_e t}}\right] \qquad (3)$$

and the diffusive event water flux ($Q_{\text{event}}^{\text{diff}}$) at time t is calculated as

$$Q_{\text{event}}^{\text{diff}} = -D_e \frac{\partial C_{\text{event}}}{\partial z}\bigg|_{z=0} = \sqrt{\frac{D_e}{\pi t}}, \qquad (4)$$

where erfc[ ] represents the complementary error function. The average diffusive event water flux during the precipitation event, over the event duration T, is then obtained as the following:

$$\bar{Q}_{\text{event}}^{\text{diff}} = \int_0^T Q_{\text{event}}^{\text{diff}} dt \bigg/ \int_0^T dt = \sqrt{\frac{4 D_e}{\pi T}}. \qquad (5)$$

[23] For the schematic hillslope identical to that used by *Jones et al.* [2006], considering a saturated sand with a porosity of 0.37, a tortuosity equal to 1.0 for simplicity, and a free solution diffusion coefficient equal to $1.2 \times 10^{-9} \text{ m}^2 \text{ s}^{-1}$, the diffusive event water flux for a 1 h precipitation event with an intensity of 10 mm h^{-1}, is

$$\bar{Q}_{\text{event}}^{\text{diff}} = \sqrt{\frac{4 \times 0.37 \times 1 \times 1.2 \times 10^{-9} \text{ m}^2 \text{ s}^{-1}}{\pi \times 3600 \text{ s}}} \approx 1.43 \text{ mm h}^{-1}$$

and thus,

$$\bar{Q}_{\text{event}}^{\text{diff}} / \bar{Q}_{\text{event}} \approx 14.3\%.$$

When the event water diffuses into the subsurface for four additional hours after a 1 h precipitation event (as analyzed by *Jones et al.* [2006]), $\bar{Q}_{\text{event}}^{\text{diff}} \approx 0.64 \text{ mm h}^{-1}$, $\bar{Q}_{\text{event}} = 2 \text{ mm h}^{-1}$, and $\bar{Q}_{\text{event}}^{\text{diff}} / \bar{Q}_{\text{event}} \approx 32\%$. Note that the numerical simulation by *Jones et al.* [2006] indicated that the pre-event water contribution would be 54.6 L (28.4%) of the total discharge (192.5 L) for the case with diffusion but no mechanical dispersion. For this study, the amount of event water that diffuses into the subsurface is $\int_{20 \text{ m}^2} \int_{5 \text{ h}} Q_{\text{event}}^{\text{diff}} dt dA = 64 \text{ L}$. This analytical estimation of the diffusive exchange of water molecules is higher than in the numerical experiment of *Jones et al.* [2006] because their event water fraction in the surface-flow regime decreased with time. However, both in the numerical and analytical analyses, diffusion can replace ~30% of the event water in the overland domain with pre-event water (28.4% in the work of *Jones et al.* [2006] and 33.2% in the analytical estimates). Therefore, the diffusion is a significant process for event and pre-event contribution to stream discharge. Note again that consideration of only the diffusion

represents the minimal mixing between event and pre-event waters and enhanced mixing can be expected with surface and subsurface flow and mechanical dispersion. This significant mixing by diffusion only implies that insignificant pre-event contribution to stream discharge may not be observable during and shortly after precipitation.

3.4. Effects of Macropore Flow

[24] The effects of macropore flow are again assessed by using the dual-permeability conceptualization described in section 2.2. Table 2 summarizes and compares the results from the single- and dual-continuum simulations. The results indicate that infiltration can increase due to the higher bulk hydraulic conductivity in the dual-continuum model, thus increasing subsurface storage, and consequently it reduces the infiltration-excess overland flow. It needs to be pointed out here that the groundwater base flow contribution to stream discharge increases but the contribution by infiltration-excess overland flow to the stream discharge decreases with more permeable subsurface materials. Thus, the overall decrease in stream discharge in the dual-continuum simulations implies that the direct surface runoff generally contributes more to the stream discharge than the subsurface base flow.

[25] It is notable in Table 2 that the ratio of the event water discharge to the total stream discharge is slightly higher but the amount of exfiltration ($\bar{Q}_{\text{exfil}}$) is significantly increased in the dual-continuum simulations. This indicates that the exfiltration is primarily derived from the event water that has infiltrated from the overland domain and that the subsurface flow component contains more event water than pre-event water near the stream. From the results, it is concluded that the groundwater ridging in a system containing macropores can further enhance subsurface flow and mixing processes but it may not enhance the relative pre-event water contribution to the stream discharge compared to the event water contribution.

4. Summary and Conclusions

[26] The hydrological response along two vertical cross sections in a hypothetical catchment to precipitation was analyzed and quantified in terms of the temporal origins and the mechanical carriers of water parcels. It was shown that the hydrological processes affecting streamflow could be significantly different in the two cross sections parallel and perpendicular to a stream. Numerical simulations of the mechanically driven flow and hydrodynamic mixing processes along the stream indicates that precipitation events can significantly enhance subsurface flow, and that event-induced subsurface flow can become relatively strong compared to regional groundwater flow inputs. However, as precipitation becomes more intense, pre-event subsurface flow components tend to be less significant contributions to the stream discharge because precipitation also enhances surface runoff and hence the event water contributions. The diffusive exchange of water molecules having different origins is interpreted to be a significant mechanism for explaining the preponderance of pre-event water in the stream, as was also shown by *Jones et al.* [2006]. The results imply that the use of tracer signals measured in a stream may be problematic to quantify the mechanically

driven quantity of water entering a stream, such as piston flow, during a precipitation event. The influence of macropore flow, evaluated via a dual-permeability conceptualization, may enhance pre-event contributions to stream discharge, but its influence is limited as the precipitation becomes more intense because the total stream discharge increases proportionally more with an intense event due to the additional surface runoff.

[27] An analysis of catchment response to precipitation along a cross section across the stream showed that most precipitation water would infiltrate slowly to the saturated zone, increasing the water storage in the subsurface. It was also shown that most of the base flow in the stream is generated through saturated groundwater flow. Event-induced groundwater ridging generates mechanical flow and also accelerates the mixing processes [*Cloke et al.*, 2006]. Interestingly, when exfiltration is generated by subsurface water discharge to a stream because of the strong groundwater ridging, the ratio of pre-event to event contributions to stream discharge becomes smaller.

[28] The following conclusions are drawn from this study:

[29] 1. Fully integrated surface and subsurface models can capture the manner in which precipitation enhances shallow saturated subsurface flow and groundwater ridging phenomena in the capillary zone near a stream in a catchment;

[30] 2. For cases in which tracer signals in the stream are strongly affected by irreversible mixing processes, the deconvolution of the signals to deduce purely mechanical flow components will be problematic;

[31] 3. Molecular diffusion is an important mechanism for the mixing of water parcels with different temporal origins and a significant amount of pre-event water discharge may be accounted for by mixing processes;

[32] 4. Capillary-fringe groundwater ridging can enhance subsurface groundwater flow near the stream, depending on the depth to the water table, the initial thickness of the capillary fringe, hydraulic conductivity, rain intensity, etc. [*Cloke et al.*, 2006], and can also accelerate the mixing between event and pre-event water parcels. The mechanical subsurface flow and hydrodynamic mixing induced by capillary-fringe groundwater ridging become stronger with more intense precipitation; however, the enhanced mixing and mechanical subsurface flow are weak contributions to streamflow compared to that of surface runoff generated by the intense precipitation.

[33] 5. Strong pre-event discharge in the stream after a precipitation event is likely due to multiple physical and chemical processes such as diffusive and mechanical mixing, the effects of macropores, and capillary fringe groundwater ridging rather than one single mechanism.

[34] It is noted that the simulations performed in this study were not intended to thoroughly explore the consequences of each of the physical and chemical processes under a broad range of conditions, but instead to demonstrate their relative significance for the redistribution of event and pre-event waters during and after an event in a simplified catchment. It is suggested that the effects of factors such as topography, geomorphology, surface and subsurface heterogeneity, initial conditions, and precipitation patterns be thoroughly analyzed in order to understand site-specific processes [*Cardenas*, 2007; *Fiori and Russo*, 2007].

References

Abdul, A. S., and R. W. Gillham (1989), Field studies of the effect of the capillary fringe on streamflow generation, *J. Hydrol.*, *112*, 1–18.

Bear, J. (1972), *Dynamics of Fluids in Porous Media*, 764 pp., Elsevier, New York.

Barenblatt, G. I., I. P. Zheltov, and I. N. Kochina (1960), Basic concepts in the theory of seepage of homogeneous liquids in fissured rocks, *J. App. Math.*, *24*, 1286–1303.

Botter, G., E. Bertuzzo, and A. Rinaldo (2010), Transport of the hydrologic response: Travel time distributions, soil moisture dynamics, and the old water paradox, *Water Resour. Res.*, *46*, W03514, doi:10.1029/2009WR008371.

Brookfield, A. E., E. A. Sudicky, Y.-J. Park, and B. Conant Jr. (2009), Simulation of thermal stream loadings using a fully-integrated surface/subsurface modeling framework, *Hydrol. Processes*, *23*, 2150–2164, doi:10.1002/hyp.7282.

Burns, D. A., J. J. McDonnell, R. P. Hooper, N. E. Peters, J. E. Freer, C. Kendall, and K. Beven (2001), Quantifying contributions to storm runoff through end-member mixing analysis and hydrologic measurements at the Panola Mountain research watershed (Georgia, USA), *Hydrol. Processes*, *15*, 1903–1924.

Cardenas, M. B. (2007), Potential contribution of topography-driven reginal groundwater flow to fractal stream chemistry: Residence time distribution analysis of Tóth flow, *Geophys. Res. Lett.*, *34*, L05403, doi:10.1029/2006GL029126.

Cloke, H. L., M. G. Anderson, J. J. McDonnell, and J.-P. Renaud (2006), Using numerical modelling to evaluate the capillary fringe groundwater ridging hypothesis of streamflow generation, *J. Hydrol.*, *316*, 141–162.

Domenico, P. A., and F. W. Schwartz (1998), *Physical and Chemical Hydrogeology*, 2nd ed., 528 pp., John Wiley, New York.

Ebel, B. A., K. Loague, W. E. Dietrich, D. R. Mongomery, R. Torres, S. P. Anderson, and T. W. Giambelluca (2007a), Near-surface hydrologic response for a steep, unchanneled catchment near Coos Bay, Oregon: 1. Sprinkling experiments, *Am. J. Sci.*, *307*, 678–708, doi:10.2475/04.2007.02.

Ebel, B. A., K. Loague, J. E. VanderKwaak, W. E. Dietrich, D. R. Mongomery, R. Torres, and S. P. Anderson (2007b), Near-surface hydrologic response for a steep, unchanneled catchment near Coos Bay, Oregon: 2. Physics-based simulations, *Am. J. Sci.*, *307*, 709–748, doi:10.2475/04.2007.03.

Fiori, A., and D. Russo (2007), Numerical analysis of subsurface flow in a steep hillslope under rainfall: The role of the spatial heterogeneity of the formation hydraulic properties, *Water Resour. Res.*, *43*, W07445, doi:10.1029/2006WR005365.

Gerke, H. H., and M. T. van Genuchten (1993), A dual-porosity model for simulating the preferential movement of water and solutes in structured porous media, *Water Resour. Res.*, *29*(2), 305–319.

Gillham, R. W. (1984), The capillary fringe and its effects on water-table response, *J. Hydrol.*, *67*, 307–324.

Jones, J. P., E. A. Sudicky, A. E. Brookfield, and Y.-J. Park (2006), An assessment of the tracer-based approach to quantifying groundwater contributions to streamflow, *Water Resour. Res.*, *42*, W02407, doi:10.1029/2005WR004130.

Jones, J. P., E. A. Sudicky, and R. G. MaLaren (2008), Application of a fully-integrated surface-subsurface flow model at watershed-scale: A case study, *Water Resour. Res.*, *44*, W03407, doi:10.1029/2006WR005603.

Kirchner, J. W. (2003), A double paradox in catchment hydrology and geochemistry, *Hydrol. Processes*, *17*, 871–874.

Larsbo, M., S. Roulier, F. Stenemo, R. Kasteel, and N. Jarvis (2005), An improved dual-permeability model of water flow and solute transport in the vadose zone, *Vadose Zone J.*, *4*, 398–406.

Li, Q., A. J. A. Unger, E. A. Sudicky, D. Kassenaar, E. J. Wexler, and S. Shikaze (2008), Predicting the multi-seasonal response of a large-scale watershed with a 3D physically-based hydrologic model, *J. Hydrol.*, *357*(3–4), 317–336.

Loague, K., and J. E. VanderKwaak (2002), Simulating hydrological response for the R-5 catchment: Comparison of two models and the impact of roads, *Hydrol. Processes*, *16*(5), 1015–1032.

Loague, K., and J. E. VanderKwaak (2004), Physics-based hydrologic response simulation: Platinum bridge, 1958 Edsel, or useful tool?, *Hydrol. Processes*, *16*(5), 1015–1032.

Loague, K., C. S. Heppner, R. H. Abrams, A. E. Carr, J. E. VanderKwaak, and B. A. Ebel (2005), Further testing of the Integrated Hydrology Model (InHM): Event-based simulations for a small rangeland catchment located near Chickasha, Oklahoma., *Hydrol. Processes*, *19*(7), 1373–1398.

Loague, K., C. S. Heppner, B. B. Mirus, B. A. Ebel, A. E. Carr, S. H. BeVille, and J. E. VanderKwaak (2006), Physics-based hydrologic-response simulation: Foundation for hydroecology and hydrogeomorphology, *Hydrol. Processes*, *20*, 1231–1237.

McDonnell, J. J. (1990), A rationale for old water discharge through macropores in a steep, humid catchment, *Water Resour. Res.*, *26*, 2821–2832.

McGlynn, B. L., and J. J. McDonnell (2003), Quantifying the relative contributions of riparian and hillslope zones to catchment runoff, *Water Resour. Res.*, *39*(11), 1310, doi:10.1029/2003WR002091.

Renaud, J.-P., H. L. Cloke, and M. Weiler (2007), Comment on "An assessment of the tracer-based approach to quantifying groundwater contributions to streamflow," by J. P. Jones et al., *Water Resour. Res.*, *43*, W09601, doi:10.1029/2006WR005157.

Schwartz, F. W., and H. Zhang (2003), *Fundamentals of Groundwater*, 592 pp., John Wiley, New York.

Sklash, M. G., and R. N. Farvolden (1979), The role of groundwater in storm runoff, *J. Hydrol.*, *43*, 45–65.

Sudicky, E. A. (1986), A natural gradient experiment on solute transport in a sand aquifer: Spatial variability of hydraulic conductivity and its role in the dispersion process, *Water Resour. Res.*, *22*, 2069–2082.

Sudicky, E. A., J. P. Jones, A. E. Brookfield, and Y.-J. Park (2007), Reply to comment by J.-P. Renaud et al. on "An assessment of the tracer-based approach to quantifying groundwater contributions to streamflow," *Water Resour. Res.*, *43*, W09602, doi:10.1029/2006WR005416.

Sudicky, E. A., J. P. Jones, Y.-J. Park, A. E. Brookfield, and D. Colautti (2008), Simulating complex flow and transport dynamics in an integrated surface-subsurface modeling framework. *Geosci. J.*, *12*(2), 107–122.

Therrien, R., R. G. McLaren, E. A. Sudicky and S. M. Panday (2003), HydroGeoSphere: A three-dimensional numerical model describing fully-integrated subsurface and surface flow and solute transport, 322 pp., Groundwater Simul. Group, Univ. Waterloo, Ontario, Canada.

Tóth, J. (1963), A theoretical analysis of groundwater flow in small drainage basin, *J. Geophys. Res.*, *67*, 4812–4975.

Turcke, M. A. and B. H. Kueper (1996), Geostatistical analysis of the Borden hydraulic conductivity field, *J. Hydrol.*, *178*(1–4), 223–240.

Unger, A. J. A., P. A. Forsyth, and E. A. Sudicky (1996), Variable spatial and temporal weighting schemes for use in multi-phase compositional problems, *Adv. Water Resour.*, *19*(1), 1–27.

VanderKwaak, J. E. (1999), Numerical simulation of flow and chemical transport in integrated surface-subsurface systems, Ph.D thesis, 242 pp., University of Waterloo, Ontario, Canada.

Van Leer, B. (1974), Towards the ultimate conservative difference scheme: II. Monotonicity and conservation combined in a second order scheme, *J. Comp. Phys.*, *14*, 361–370.

Weiler, M., and F. Naef (2003), An experimental tracer study of the role of macropores in infiltration in grassland soils, *Hydrol. Processes*, *17*, 477–493.

Weiler, M., S. Scherrer, F. Naef, and P. Burlando (1999), Hydrograph separation of runoff components based on measuring hydraulic state variables, tracer experiments, and weighting methods, *IAHS Publ. No. 258*, 249–255.

A. E. Brookfield, Kansas Geological Survey, University of Kansas, 1930 Constant Ave., Lawrence, KS 66047, USA.

J. P. Jones, Y.-J. Park, and E. A. Sudicky, Department of Earth and Environmental Sciences, University of Waterloo, 200 University Ave. W, Waterloo, ON N2L 3G1, Canada. (yj2park@sciborg.uwaterloo.ca)